



OPEN ACCESS

EDITED BY
Simone Cauzzo,
University of Padua, Italy

REVIEWED BY
Jiaxing Wang,
Columbia University, United States
Akanksha Kaushik,
The NorthCap University School of
Engineering & Technology, India

*CORRESPONDENCE
Lei Wang
✉ lei.wang@nkcswx.cn

RECEIVED 09 June 2025
ACCEPTED 30 June 2025
PUBLISHED 22 July 2025

CITATION
Huang Z and Wang L (2025) The role of IP₃ receptors and SERCA pumps in restoring working memory under amyloid β induced Alzheimer's disease: a modeling study. *Front. Comput. Neurosci.* 19:1643547. doi: 10.3389/fncom.2025.1643547

COPYRIGHT
© 2025 Huang and Wang. This is an open-access article distributed under the terms of the [Creative Commons Attribution License \(CC BY\)](#). The use, distribution or reproduction in other forums is permitted, provided the original author(s) and the copyright owner(s) are credited and that the original publication in this journal is cited, in accordance with accepted academic practice. No use, distribution or reproduction is permitted which does not comply with these terms.

The role of IP₃ receptors and SERCA pumps in restoring working memory under amyloid β induced Alzheimer's disease: a modeling study

Ziyi Huang and Lei Wang*

Scholastic Excellence Research Center, Wuxi Dipont School of Arts and Science, Wuxi, China

Memory impairment is a prevalent symptom in patients with Alzheimer's disease (AD), with working memory loss being the most prominent deficit. Recent experimental evidence suggests that abnormal calcium levels in the Endoplasmic Reticulum (ER) may disrupt synaptic transmission, leading to memory loss in AD patients. However, the specific mechanisms by which intracellular calcium homeostasis influences memory formation, storage, and recall in the context of AD remain unclear. In this study, we investigate the effects of intracellular calcium homeostasis on AD-related working memory (WM) using a spiking network model. We quantify memory storage by measuring the similarity between images during the training and testing phases. The model results indicate that ~90% of memory can be stored in the WM network under normal conditions. In contrast, the presence of amyloid beta ($A\beta$), associated with AD, significantly reduces this similarity, allowing only 54%-58% of memory to be stored, this alteration trend is consistent with previous experimental findings. Further analysis reveals that downregulating the activation of inositol triphosphate (IP₃) receptors and upregulating the activation of the sarco-endoplasmic reticulum Ca²⁺ ATPase (SERCA) pumps can enhance memory performance, achieving about 78% and 77%, respectively. Moreover, simultaneously manipulating both IP₃ and SERCA activations can increase memory capacity to around 81%. These findings suggest several potential therapeutic targets for addressing memory impairment in $A\beta$ aggregation induced AD patients. Additionally, our network model could serve as a foundation for exploring further mechanisms that modulate memory dysfunction at the genetic, cellular, and network levels.

KEYWORDS

working memory, Alzheimer's disease, spiking network, IP₃ receptors, SERCA pumps

1 Introductions

Alzheimer's disease (AD) is the most prevalent neurodegenerative disorder and the leading cause of dementia worldwide. It is affecting more than 40 million people globally, as this number is constantly increasing (Kim et al., 2024). AD is commonly associated with the accumulation of amyloid-beta ($A\beta$) plaques and tau tangles. Cognitive symptoms such as working memory (WM) loss are often detected before these pathological hallmarks (Breijyeh and Karaman, 2020). The early dysfunction of working memory (i.e., the ability to temporarily store and process information) shows that defects in neuronal pathways may result in the initial cognitive deficits before the major neurodegenerations occur.

Recent advances in neuroscience research demonstrate that astrocyte, the previously considered supporting cell (Kimelberg and Nedergaard, 2010; Farhy-Tselnicker and Allen, 2018), plays an important role in WM via synapse modulations (Gordleeva et al., 2021). Astrocytes respond to neuronal activities by producing intracellular inositol triphosphate (IP_3), causing calcium (Ca^{2+}) release from internal stores. The Ca^{2+} elevation triggers the increase of gliotransmitters release, which enhances the synaptic connections, forming the basis of short-term memory formation. This feedback loop has been tested to successfully model the encoding and retrieval of WM under a biologically plausible network (Gordleeva et al., 2021).

However, this intricate mechanism became vulnerable in the situation of AD. $A\beta$ oligomers is studied to interfere with intracellular Ca^{2+} homeostasis by enhancing membrane leak, over-activating IP_3 receptors and suppressing the activity of sarcoplasmic reticulum Ca^{2+} ATPase (SERCA) pumps, leading to persistent intracellular Ca^{2+} elevation and signaling irregularities (Latulippe et al., 2018). This abnormality leads to the unstable intracellular environment while also impairs the astrocytic capacity on modulating working memory, which might be the reason of WM damage.

Most research on the causes and treatments of AD has been conducted through experimental methods, which are often rigorous and time-consuming. Given this challenge, computational approaches have emerged as a viable alternative (Moravveji et al., 2024). In recent decades, numerous network models have been developed to explore potential mechanisms related to the causes and treatments of AD, addressing areas such as disease progression (Chamberland et al., 2024; Bertsch et al., 2017), pathogenesis (Puri and Li, 2010), the effects of specific proteins (Helal et al., 2019, 2014), and mitochondrial dysfunction (Toglia et al., 2018). Many of these studies have utilized non-spiking neuron models; however, spiking signals are intrinsic to neurons and can be reliably transmitted over long distances in brain regions affected by AD. Therefore, this study employs spiking neuron models as the primary functional units in constructing the network.

In this study, we construct a computational network model to examine how intracellular calcium homeostasis affects the formation, impairment, and restoration of WM under $A\beta$ -induced AD conditions. The network comprises two cell types: spiking excitatory neurons and non-spiking astrocytes. The neurons are primarily responsible for generating population spiking activity, while the astrocytes are mainly involved in producing various calcium signals. Model results indicate that the presence of $A\beta$ impairs WM performance by significantly increasing Ca^{2+} concentrations. Conversely, downregulating IP_3 activation and upregulating SERCA activation, either separately or simultaneously, can help restore WM performance to some extent.

2 Model descriptions

In this study, we introduce a biologically plausible spiking neuron-astrocyte network that simulates WM through local synaptic modulations. Neurons generate spikes in response to external stimuli, releasing glutamates into the extracellular space. Surrounding astrocytes detect these glutamates, activating internal

IP_3 and Ca^{2+} signaling cascades. When astrocytic Ca^{2+} exceeds a critical threshold, gliotransmitters are released, transiently enhancing synaptic weights in the stimulated neuronal subnetwork. This temporary potentiation supports cue-based memory retrieval during test phases. In the following subsections, we detail the model components responsible for simulating this loop, including the neuron dynamics, astrocyte calcium signaling, $A\beta$ modulation, and memory performance metrics.

Architecture and cell units of our network model are inspired and adapted from Gordleeva et al. (2021). Based on the spiking network, we employed three additional elements: $A\beta$ -dependent calcium flows, calcium-dependent variations of synaptic weight combined with $A\beta$ modulations, and negative components in describing the activation of IP_3 . The first two elements are used to introduce the influence of $A\beta$. The larger the $A\beta$ value, the more severe the AD and the worse the WM performance. The last element is used to balance the variation of IP_3 .

2.1 Neuron model

Spiking dynamics of single neuron is described using the Izhikevich model (Izhikevich, 2003). Due to its simplicity and computational efficient, this neuron model has been widely used to study population activities of neurons, e.g., synchronization and oscillation (Khoshkhou and Montakhab, 2018).

Mathematical expressions of the Izhikevich model are:

$$\begin{aligned} \frac{dV(i,j)}{dt} &= 0.04(V(i,j))^2 + 5V(i,j) - U(i,j) + 140 + I_{app}(i,j) \\ &\quad + I_{syn}(i,j) \\ \frac{dU(i,j)}{dt} &= a(bV(i,j) - U(i,j)) \end{aligned} \quad (1)$$

with the auxiliary after-spike resetting:

$$\text{if } V(i,j) \geq 30 \text{ mV, then } \begin{cases} V(i,j) \leftarrow c \\ U(i,j) \leftarrow U(i,j) + d \end{cases} \quad (2)$$

Here, V represents the transmembrane potential, while U denotes a membrane recovery variable that provides negative feedback to V . The indices (i, j) indicate the corresponding neuron. c is the resting potential, and a, b, d are dimensionless parameters. I_{app} refers to the applied currents to the respective neurons, which will be explained further below.

Synaptic currents that neurons receive is expressed as Gordleeva et al. (2021):

$$I_{syn}(i,j) = \sum_{k=1}^{N(i,j)} \frac{g_{syn}(i,j)(E_{syn} - V(i,j))}{1 + \exp\left(-\frac{V_{pre}^k}{k_{syn}}\right)} \quad (3)$$

Here, N is the total number of presynaptic neurons, E_{syn} is the reversal potential for the synapse, V_{pre} denotes the membrane potential of the presynaptic neuron, and k_{syn} is slope of the synaptic activation function. The parameter g_{syn} describes the synaptic strength (Gordleeva et al., 2021):

$$g_{syn}(i,j) = \eta + v_{ca}(m, n) \quad (4)$$

TABLE 1 Parameter values in the neuron model.

| Parameter | Description | Value |
|-----------|--|--------|
| a | Time scale of the recovery variable | 0.1 |
| b | Sensitivity of the recovery variable to the subthreshold fluctuation of membrane potential | 0.2 |
| c | After-spike reset value of the membrane potential | -65 mV |
| d | After-spike reset of the recovery variable | 2 |
| N | Number of input connections per each neuron | 40 |
| η | Synaptic weight without astrocyte inputs | 0.025 |
| E_{syn} | Synaptic reversal potential for excitatory synapse | 0 mV |
| k_{syn} | Slope of the synaptic activation function | 0.2 mV |

Here (m, n) denotes the index of the corresponding astrocyte that modulates the synaptic currents of neuron (i, j) . η represents the synaptic weight without astrocyte influence, while v_{ca} denotes the astrocyte-induced modulation of synaptic strength.

Specific values of these parameters are given in Table 1.

2.2 Astrocyte model

As mentioned above, astrocytes in our network primarily generate various calcium signals. Following the method used in the previous study (Gordleeva et al., 2021), a mean-field approach is employed to describe the emergence of Ca^{2+} signals, as shown in Equation 5 and Figure 1.

$$\begin{aligned} \frac{d[Ca^{2+}](m, n)}{dt} &= J_{ER}(m, n) - J_{pump}(m, n) + J_{leak}(m, n) \\ &\quad + J_{in}(m, n) - J_{out}(m, n) + df_{Ca}(m, n) \\ \frac{dh(m, n)}{dt} &= a_2 \left(d_2 \frac{IP_3(m, n) + d_1}{IP_3(m, n) + d_3} (1 - h(m, n)) \right. \\ &\quad \left. - [Ca^{2+}](m, n) h(m, n) \right) \end{aligned} \quad (5)$$

Here Ca^{2+} indicate the intracellular calcium concentration, h is the fraction of the activated IP_3 receptors on the ER surface. Detailed expressions of each flux are:

$$\begin{aligned} J_{ER} &= c_1 v_1 [Ca^{2+}]^3 h^3 IP_3^3 \frac{(c_0/c_1 - (1 + 1/c_1) [Ca^{2+}])}{((IP_3 + d_1) ([Ca^{2+}] + d_5))^3} \\ J_{pump} &= \gamma \frac{v_3 [Ca^{2+}]^2}{k_3^2 + [Ca^{2+}]^2} \\ J_{leak} &= c_1 v_2 (c_0/c_1 - (1 + 1/c_1) [Ca^{2+}]) \\ J_{in} &= \frac{v_6 IP_3^2}{k_2^2 + IP_3^2} + v_x \\ J_{out} &= k_1 [Ca^{2+}] \end{aligned} \quad (6)$$

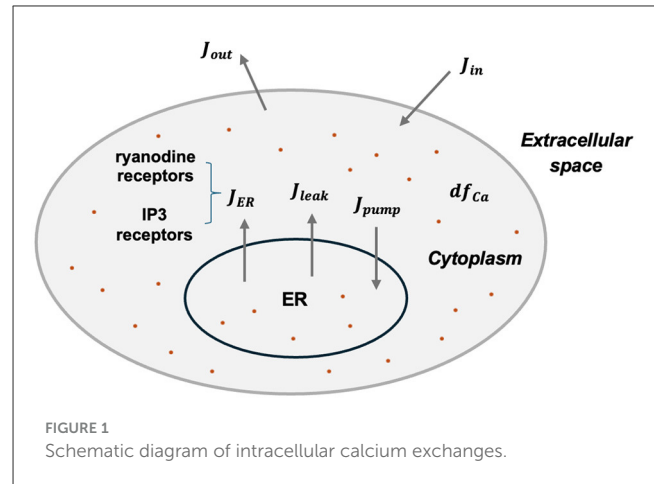


FIGURE 1 Schematic diagram of intracellular calcium exchanges.

Here J_{ER} represents the Ca^{2+} flux from the ER to the cytoplasm through IP_3 receptors and ryanodine receptors (RyR). J_{pump} denotes the Ca^{2+} flux pumped back into the ER via the SERCA, while J_{leak} indicates the leakage flux from the ER to the cytoplasm. J_{in} and J_{out} describe the calcium exchange with extracellular space.

Activation dynamics of IP_3 is expressed as Gordleeva et al. (2021) and Wagner et al. (2004):

$$\begin{aligned} \frac{dIP_3(m, n)}{dt} &= \frac{IP_3^* - IP_3(m, n)}{\tau_{IP_3}} + \lambda (J_{PLC\delta}(m, n) + J_{glu}(m, n)) \\ &\quad + df_{IP_3}(m, n) - kv_4 \frac{J_{Kinase}(m, n) - J_{Phosphatase}(m, n)}{\lambda} \end{aligned} \quad (7)$$

Here IP_3^* denotes the steady-state concentration of the IP_3 receptors, while τ_{IP_3} is the rate constant for IP_3 loss. λ is a control parameter used to regulate various elements in IP_3 dynamics. $J_{PLC\delta}$ describes the production of IP_3 by phospholipase C8 (PLC8), expressed as Gordleeva et al. (2021):

$$J_{PLC\delta} = \frac{v_4 ([Ca^{2+}] + (1 - \alpha) k_4)}{[Ca^{2+}] + k_4} \quad (8)$$

J_{glu} describes the production of IP_3 induced by glutamate in response to neuronal activities, which is modeled as Gordleeva et al. (2021):

$$J_{glu} = \begin{cases} A_{glu}, & \text{if } t_0 < t \leq t_0 + t_{glu} \\ 0, & \text{otherwise} \end{cases} \quad (9)$$

Here A_{glu} represents the amplitude of glutamate contributing to the production of IP_3 , while t_{glu} denotes the periods when the total level of glutamate from all synapses reaches a given threshold:

$$\left(\frac{1}{N_a} \sum_{(i,j) \in N_a} [G(i,j) > G_{thr}] \right) > F_{act} \quad (10)$$

Here N_a represents the number of neurons connected to a single astrocyte, $G_{thr} = 0.7$ is the threshold, and $[x]$ denotes the Iverson bracket. $F_{act} = 0.5$ indicates the fraction of synchronously

spiking neurons within the total neuronal ensemble associated with the astrocyte. G refers to the amount of glutamate, which will be explained further below.

J_{Kinase} and $J_{Phosphatase}$ are currents for IP_3 degradation, which are expressed as [Wagner et al. \(2004\)](#):

$$J_{Kinase} = (1 - \rho) kv_1 \frac{IP_3}{IP_3 + 2.5} + \rho \cdot kv_2 \frac{IP_3}{IP_3 + 0.5} \quad (11)$$

$$J_{Phosphatase} = kv_3 \frac{IP_3}{IP_3 + 30} \quad (12)$$

$$\rho = \frac{[Ca^{2+}]}{[Ca^{2+}] + 0.39} \quad (13)$$

The currents df_{Ca} in [Equation 5](#) and df_{IP_3} in [Equation 7](#) represent the diffusion of Ca^{2+} ions and IP_3 molecules via gap junctions between astrocytes, expressed as follows ([Gordleeva et al., 2021](#)):

$$\begin{aligned} df_{Ca}(m, n) &= d_{Ca} (\Delta [Ca^{2+}]) (m, n) \\ df_{IP_3}(m, n) &= d_{IP_3} (\Delta IP_3) (m, n) \end{aligned} \quad (14)$$

Here d_{Ca} and d_{IP_3} represent the diffusion rate of the Ca^{2+} and IP_3 , respectively. Following a previous study ([Gordleeva et al., 2021](#)), we assume that each astrocyte is diffusively coupled only with its four nearest neighbors:

$$\begin{aligned} (\Delta [Ca^{2+}]) (m, n) &= (\Delta [Ca^{2+}]) (m + 1, n) \\ &+ (\Delta [Ca^{2+}]) (m - 1, n) \\ &+ (\Delta [Ca^{2+}]) (m, n + 1) \\ &+ (\Delta [Ca^{2+}]) (m, n - 1) - 4 (Ca^{2+}) (m, n) \end{aligned} \quad (15)$$

$$\begin{aligned} (\Delta IP_3) (m, n) &= (\Delta IP_3) (m + 1, n) + (\Delta IP_3) (m - 1, n) \\ &+ (\Delta IP_3) (m, n + 1) + (\Delta IP_3) (m, n - 1) \\ &- 4 (IP_3) (m, n) \end{aligned} \quad (16)$$

Specific values of these parameters are given in [Table 2](#).

2.3 Neuron-astrocyte network

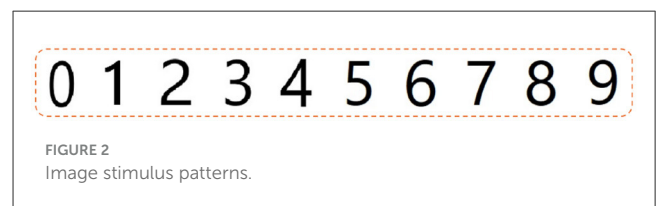
As described in [Gordleeva et al. \(2021\)](#), the network model for WM comprises three layers: the input layer, the neurons layer, and the astrocytes layer. The input layer consists of two types of stimuli: (1) image signals labeled {"0", "1", "2", "3", "4", "5", "6", "7", "8", "9"} ([Figure 2](#)), which are responsible for memory training and testing, and (2) background noise signals, that generate low-rate spontaneous spikes.

The neurons layer contains 79×79 neurons, which receive stimuli from the input layer and project to the astrocytes layer. The third layer consists of 26×26 astrocytes, with each astrocyte projecting back to neurons in the second layer.

The architecture of synaptic connections among neurons is random; specifically, each neuron connects to $N = 40$ local postsynaptic target neurons via excitatory chemical synapses, with these neurons chosen randomly from the neurons layer. In contrast, the synaptic connections among astrocytes are deterministic, with

TABLE 2 Parameter values in astrocyte model.

| Parameter | Description | Value |
|------------|--|-----------------|
| v_1 | Max Ca^{2+} flux | $6 s^{-1}$ |
| v_2 | Ca^{2+} leak flux constant | $0.11 s^{-1}$ |
| v_3 | Max Ca^{2+} uptake | $2.2 \mu M/s$ |
| v_4 | Max rate of IP_3 production | $0.3 \mu M/s$ |
| v_6 | Max rate of activation-dependent Ca^{2+} influx | $0.2 \mu M/s$ |
| v_x | Ca^{2+} influx scaling factor | $0.025 \mu M/s$ |
| c_0 | Total Ca^{2+} in the cytoplasm | $2.0 \mu M$ |
| c_1 | Ratio of ER volume to cytoplasm volume | 0.185 |
| d_1 | Dissociation constant for IP_3 | $0.13 \mu M$ |
| d_2 | Dissociation constant for Ca^{2+} inhibition | $1.049 \mu M$ |
| d_3 | Receptor dissociation constant for IP_3 | $943.4 nM$ |
| d_5 | Ca^{2+} activation constant | $82 nM$ |
| k_1 | Rate constant of Ca^{2+} extrusion | $0.5 s^{-1}$ |
| k_2 | Half-saturation constant for agonist-dependent Ca^{2+} entry | $1 \mu M$ |
| k_3 | Activation constant for ATP – Ca^{2+} pump | $0.1 \mu M$ |
| k_4 | Dissociation constant for Ca^{2+} stimulation of IP_3 production | $1.1 \mu M$ |
| kv_1 | Max rate constant at low Ca^{2+} | $0.001 \mu M/s$ |
| kv_2 | Max rate constant at high Ca^{2+} | $0.005 \mu M/s$ |
| kv_3 | Max rate constant (phosphatase) | $0.02 \mu M/s$ |
| kv_4 | IP_3 production rate scaling factor | 10/0.083 |
| IP_3^* | Steady state concentration of IP_3 | $0.16 \mu M$ |
| d_{ca} | Ca^{2+} diffusion rate | $0.05 s^{-1}$ |
| d_{IP_3} | IP_3 diffusion rate | $0.1 s^{-1}$ |
| A_{glu} | Rate of IP_3 production through glutamate | $5 \mu M/s$ |



each astrocyte connecting to its four nearest neighbors via gap junctions ([Gordleeva et al., 2021](#)).

Additionally, each astrocyte connects with $N_a = 16$ (i.e., 4×4) neurons through reciprocal excitatory chemical synapses. Thus, the synaptic strength in [Equation 4](#) has a Ca^{2+} dependent component v_{Ca} , which can be expressed as:

$$v_{Ca} = v_{Ca}^* \Theta \left([Ca^{2+}]^{(m,n)} - [Ca^{2+}]_{thr} \right) \quad (17)$$

Here v_{Ca}^* denotes the strength of astrocyte-induced modulation of synaptic weight, $\Theta(x)$ is the Heaviside step-function, and $[Ca^{2+}]_{thr}$ is the threshold.

In Equation 10, the amount of glutamate G is characterized as Gordleeva et al. (2021):

$$\frac{dG(i, j)}{dt} = -\alpha_{glu}G(i, j) + k_{glu}\Theta(V(i, j) - 30) \quad (18)$$

Here α_{glu} represents the glutamate clearance constant, while k_{glu} indicates the efficacy of the release. Similar to Equation 17, $\Theta(x)$ is the Heaviside step-function.

Specific values of relevant parameters are given in Table 3.

2.4 Stimulation protocol

Our stimulation protocol follows the delayed match-to-sample task (DMS), which is commonly used in experimental studies of memory formation and recall. During the training phase, an image labeled with a specific digit is presented for 200 ms (500 ms-700 ms), followed by a 700 ms break (700 ms-1,400 ms). After this, two non-match images are displayed, each for 150 ms (1,400 ms-1,550 ms and 1,800 ms-1,950 ms), with a 250 ms break in between (1,550 ms-1,800 ms and 1,950 ms-2,200 ms). Finally, the matching stimulus appears for 150 ms (2,200 ms-2,350 ms) to test the network’s memory recall capability. The total duration of the simulation experiment is 3,000 ms. Detailed stimulus information during training and testing phases can refer to Gordleeva et al. (2021). A demonstration of a sample stimulus current and the corresponding neuronal activities during the training and test phases is presented in Supplementary Figure 17.

2.5 Memory performance matrices

To quantify the amount of memory that can be stored, we use a measure calculated based on the similarity between a recalled image and the sample image. The similarity ranges from 0 to 1, with larger values indicating better WM performance.

$$M_{ij}(t) = I \left[\left(\sum_{k=t-w}^t I[V_{ij}(k) > thr] \right) > 0 \right]$$

$$C(t) = \frac{1}{2} \left(\frac{1}{|P|} \sum_{(ij) \in P} M_{ij}(t) + \frac{1}{W \cdot H - |P|} \sum_{(ij) \notin P} (1 - M_{ij}(t)) \right) \quad (19)$$

TABLE 3 Parameter values in neuron-astrocyte network.

| Parameter | Description | Value |
|-------------------|---|---------------------|
| N_a | Number of neurons connecting with one astrocyte | 16 |
| α_{glu} | Glutamate clearance constant | 10 s^{-1} |
| k_{glu} | Efficacy of glutamate release | $600 \mu\text{M/s}$ |
| v_{ca}^* | Strength of astrocyte-induced modulation of synaptic weight | 0.5 |
| $[Ca^{2+}]_{thr}$ | Threshold concentration of Ca^{2+} for the astrocytic modulation of synapse | $0.15 \mu\text{M}$ |

$$C_P = \frac{1}{|T_P|} \max_{t \in T_P} C(t)$$

Here $w = 1 \text{ ms}$ represents the time step, thr denotes the spiking threshold of the neuron, P is the set of pixels belonging to the sample image, and W and H are the network dimensions. I is the indicator function, and T_P is the set of frames within the tracking range of pattern P . For more details (see Gordleeva et al., 2021).

2.6 Introduction of $A\beta$ to calcium flows

The effect of $A\beta$ on calcium dynamics is reflected in its influence on the currents J_{in} and J_{ER} . Following a previous study (Latulippe et al., 2018), J_{in} and J_{ER} with the addition of $A\beta$ are expressed as:

$$J_{in} = \frac{v_6 IP_3^2}{k_2^2 + IP_3^2} + v_x + A_\beta^4$$

$$J_{ER} = c_1 v_1 [Ca^{2+}]^3 h^3 IP_3^3 \frac{(c_0/c_1 - (1 + 1/c_1) [Ca^{2+}])}{((IP_3 + d_1) ([Ca^{2+}] + d_5 + 0.02A_\beta))^3} \quad (20)$$

Here A_β represents a fixed level of $A\beta$ concentration.

2.7 Calcium-dependent change of synaptic weights with $A\beta$ modulations

Previous experimental results indicate that high concentrations of Ca^{2+} can promote the release probability of neurotransmitters, thereby strengthening synaptic connections between neurons (Neher and Sakaba, 2008). However, excessive levels of Ca^{2+} can disrupt synaptic connections by inducing irreversible excitotoxic injury (Vermma et al., 2022). In our model, Equation 21 is employed to prevent exaggerated Ca^{2+} concentrations.

$$w_a = \frac{1.2}{1 + \exp\left(\frac{1-12.1[Ca^{2+}]}{0.2}\right)} \exp(-[Ca^{2+}]) \quad (21)$$

Another experiment demonstrated that the accumulation of $A\beta$ negatively affects Ca^{2+} levels (Toglia et al., 2018). Therefore, Equation 22 is introduced to simulate this variation.

$$w_b = \begin{cases} 1 + \exp(-2A_\beta) w_a & \text{if } [Ca^{2+}] \leq 0.15 \\ \exp(-2A_\beta) w_a & \text{else} \end{cases} \quad (22)$$

Here A_β represents a fixed level of $A\beta$ concentration. Based on the value of w_b , we have $v_{Ca}^* = w_b * v_{Ca}^*$.

All simulations were performed using the Matlab software (Matlab R2021a), and the fourth-order Runge-Kutta algorithm was employed to calculate the values of different variables with a time integration step of 0.1 ms.

3 Model results

In this section, we present the functional outcomes of the neuron-astrocyte network model under both normal and AD-like conditions. We begin by illustrating how the intact system

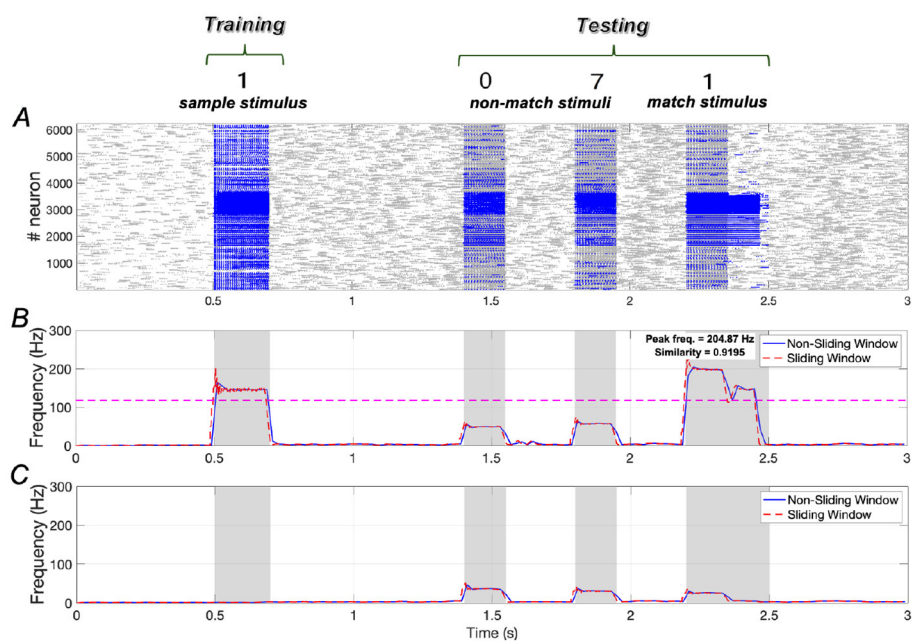


FIGURE 3

Neuronal responses in WM network under normal conditions. (A) Raster plots of spikes for all the neurons during different phases; (B, C) Average frequencies of stimulus-specific and unspecific neurons using different time windows, respectively (bin = 20 ms).

encodes, maintains, and successfully retrieves a single stimulus, highlighting the role of astrocyte-mediated synaptic modulation in WM. Next, we analyze memory performance metrics across varying levels of $A\beta$ pathology and under parameter modulations targeting IP_3 production and $SERCA$ activity. These results provide valuable insights into the effects of calcium dysregulation on WM and emphasize potential strategies for restoring cognitive function in $A\beta$ -induced AD.

3.1 WM network performance under normal conditions

In the absence of $A\beta$ (indicating no AD symptoms), the WM network performs effectively. Results shown in Figure 3 illustrate that the training stimulus “1” can be successfully recalled during the testing period after two non-match stimuli (“0” and “7”). Quantitative results in terms of similarity and peak frequency indicate that the similarity of neuronal responses to the sample stimulus and the match stimulus reaches ~ 0.9195 . Additionally, the peak frequency of neurons responding to the match stimulus is comparable to that of neurons responding to the sample stimulus.

The dotted pink line in Figure 3B is determined by evaluating each stimulus from the set {“0”, “2”, “3”, “4”, “5”, “6”, “7”, “8”, “9”} as the match stimulus and calculating the maximum peak frequency among these stimuli (see Supplementary Figure 18). If the peak frequency of neurons under the match stimulus “1” exceeds this line, we consider neuronal activity under “1” to be distinguishable from the activities elicited by the other stimuli.

Results presented in Figures 4A, B illustrate the spiking sequence of a stimulus-specific neuron along with the amount of glutamate (G) it releases, demonstrating comparable spiking activities for both the sample and match stimuli. Figures 4C, D display the Ca^{2+} signal and IP_3 levels in an astrocyte that is synaptically connected to the stimulus-specific neuron. It is evident that once the glutamate release from the neuron reaches a certain threshold (“0.7”, as indicated in Equation 10), the IP_3 level rises rapidly. This continuous increase in IP_3 concentration gradually elevates the Ca^{2+} levels, ultimately enhancing neuronal responses. These findings highlight the critical role of Ca^{2+} -mediated modulation in sustaining working memory, aligning with previous research (Mongillo et al., 2008).

3.2 WM network performance in the presence of $A\beta$

Accumulation of $A\beta$ has been linked to memory loss in AD in numerous studies (Hampel et al., 2021; Ma and Klann, 2012; Poling et al., 2008). In our research, we simulate $A\beta$ accumulation by varying the $A\beta$ parameter and observe changes in memory performance. Figure 5 illustrates how similarity and peak frequency vary with respect to $A\beta$ levels, showing that increased $A\beta$ significantly impairs WM performance. Specifically, the peak frequency decreases from over 200 Hz ($A\beta = 0$) to 93.87 Hz ($A\beta = 1.6$), while similarity drops from 0.9195 ($A\beta = 0$) to 0.541 ($A\beta = 1.6$), indicating a substantial loss of memory recall fidelity.

In the following sections, we will separately analyze how memory performance is disrupted and the potential for restoration at $A\beta = 1.2$ (mild AD) and $A\beta = 1.6$ (severe AD).

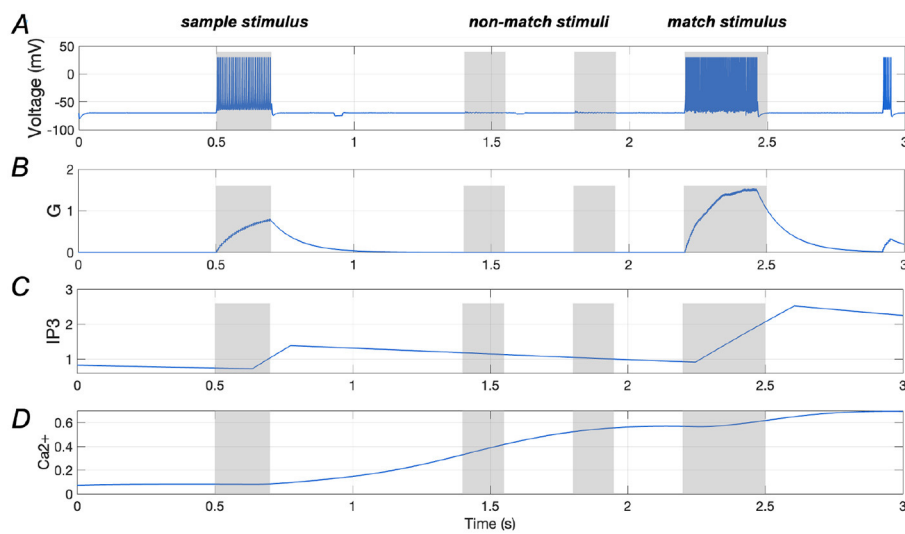


FIGURE 4 Responses of a stimulus-specific neuron and corresponding astrocyte. **(A, B)** Spike train of a specific neuron and the amount of glutamate (G) it releases, respectively; **(C, D)** Ca^{2+} signals and IP_3 value of an astrocyte which has synaptic connection with the specific neuron.

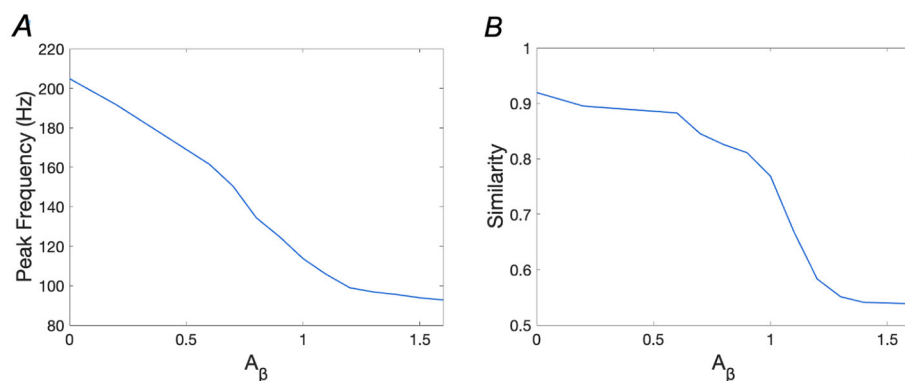


FIGURE 5 Peak frequencies and similarities with the increase of $A\beta$. **(A)** Peak Frequency vs. $A\beta$; **(B)** Similarity vs. $A\beta$.

3.2.1 Working memory impairment under mild $A\beta$ accumulation

Results shown in Figure 6 indicate that the addition of a small amount of $A\beta$ significantly impairs WM performance. Specifically, similarity decreases from 0.9195 to 0.5832, representing a reduction of ~36.6%, while peak frequency drops from 204.87 Hz to 98.98 Hz, reflecting a 51.7% reduction.

Figures 7A, B illustrate the spiking response of a stimulus-specific neuron, and the amount of glutamate released, further highlighting the negative modulatory effect of $A\beta$. Additionally, the Ca^{2+} signal and IP_3 levels in an astrocyte that is connected to the neuron are demonstrated in Figures 7C, D, in which the amplitude of Ca^{2+} signal shows an increasing trend, rising from about 0.7 (as seen in Figure 4D) to ~1.4 (as shown in Figure 7D). This finding aligns with previous studies indicating that $A\beta$ accumulation disrupts calcium homeostasis, leading to increased

Ca^{2+} concentrations in the intracellular space (Fani et al., 2021; Toglietta et al., 2018).

3.2.2 Working memory impairment under severe $A\beta$ accumulation

Results presented in Figure 8 indicate that the addition of a large amount of $A\beta$ to the network severely impairs WM performance. Specifically, similarity decreases from 0.9195 to 0.5380, representing a reduction of ~41.5%, while peak frequency declines from 204.87 Hz to 92.80 Hz, reflecting a 54.7% reduction. These decreases are more pronounced than those observed at $A\beta = 1.2$.

Figures 9A, B illustrate the spiking response of a stimulus-specific neuron along with the amount of glutamate released, further emphasizing the negative modulatory effect of $A\beta$.

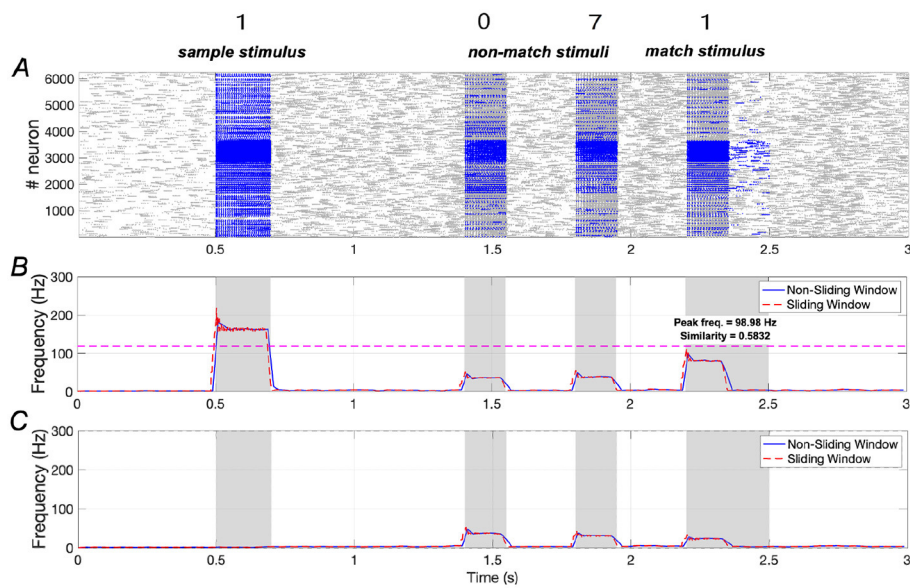


FIGURE 6 Neuronal responses in WM network in the presence of $A\beta$ ($A\beta = 1.2$). **(A)** Raster plots of spikes for all the neurons during different phases; **(B, C)** Average frequencies of stimulus-specific and unspecific neurons using different time windows, respectively (bin = 20 ms).

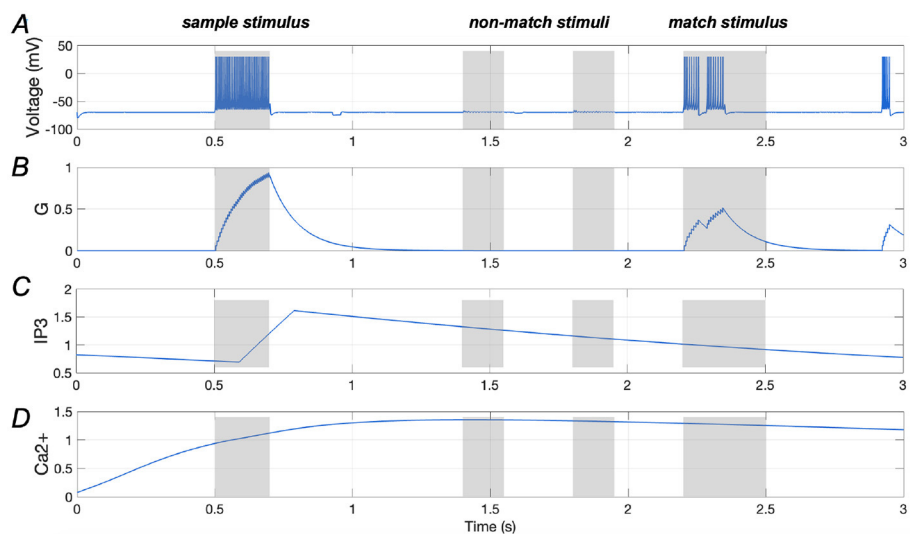


FIGURE 7 Responses of a stimulus-specific neuron and corresponding astrocyte in the presence of $A\beta$ ($A\beta = 1.2$). **(A, B)** Spike train of a specific neuron and the amount of glutamate (G) it releases, respectively; **(C, D)** Ca^{2+} signals and IP_3 values of an astrocyte which has synaptic connection with the specific neuron.

Additionally, the Ca^{2+} signal and IP_3 levels in an astrocyte that is connected to the neuron are demonstrated in **Figures 9C, D**, in which the amplitude of Ca^{2+} signal shows significant growth, reaching ~ 5 (as shown in **Figure 9D**).

3.3 Restoring WM network performance by downregulating IP_3 activation

The results in Section 3.2 indicate that excessive levels of Ca^{2+} induced by $A\beta$ play a crucial role in disrupting the memory

performance of WM network. In this section, we investigate whether downregulation of IP_3 can partially restore WM under pathological conditions by reducing intracellular calcium levels, as IP_3 positively influences intracellular calcium concentration (see **Equations 5, 6**).

In **Figure 10**, we analyze two cases under the condition of $A\beta = 1.2$ (mild AD): (1) When $\lambda = 0.1$ (see **Equation 7**), similarity increases from 0.5832 to 0.7752, a rise of $\sim 32.9\%$, and peak frequency increases from 98.98 Hz to 115.36 Hz, reflecting a 16.5% increase; (2) When $\lambda = 0.05$, similarity rises from 0.5832 to 0.7808, representing a 33.9% increase, while peak

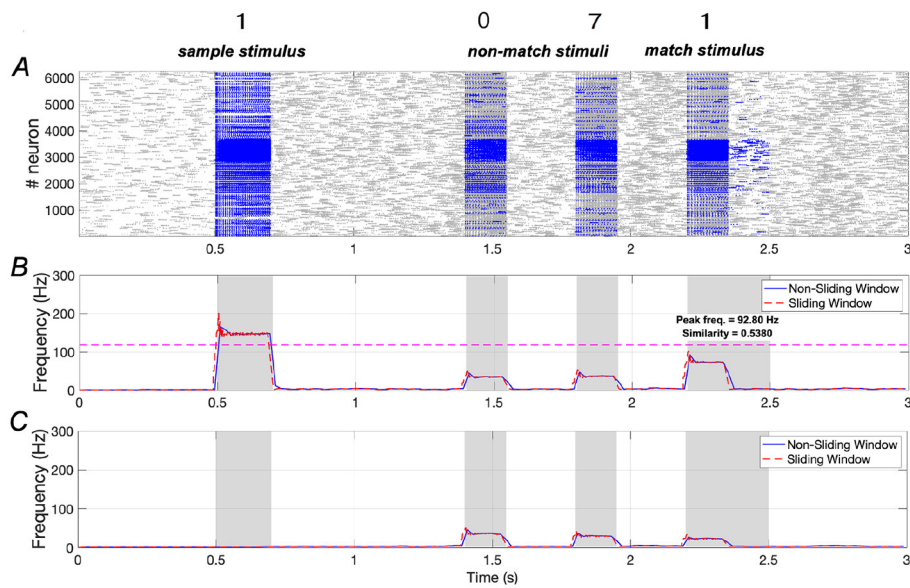


FIGURE 8 Neuronal responses in WM network in the presence of $A\beta$ ($A\beta = 1.6$). **(A)** Raster plots of spikes for all the neurons during different phases; **(B, C)** Average frequencies of stimulus-specific and unspecific neurons using different time windows, respectively (bin = 20 ms).

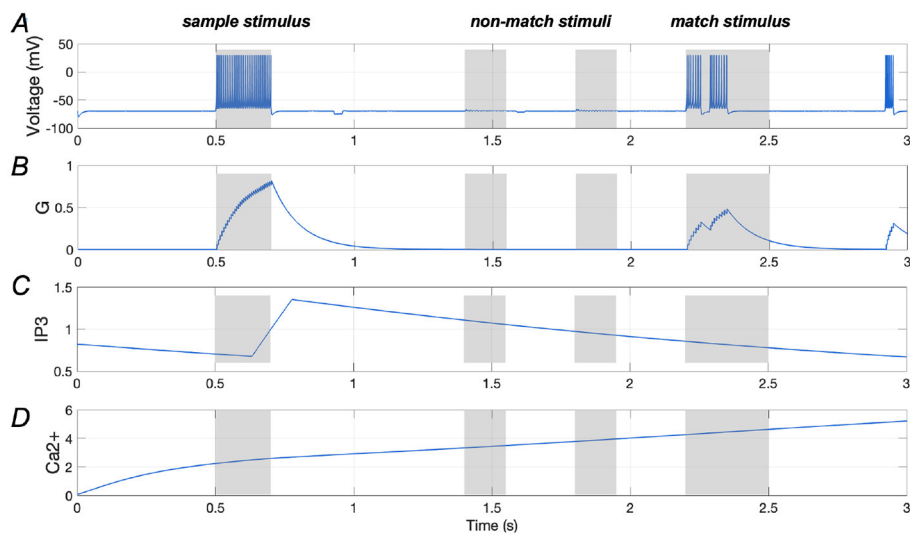


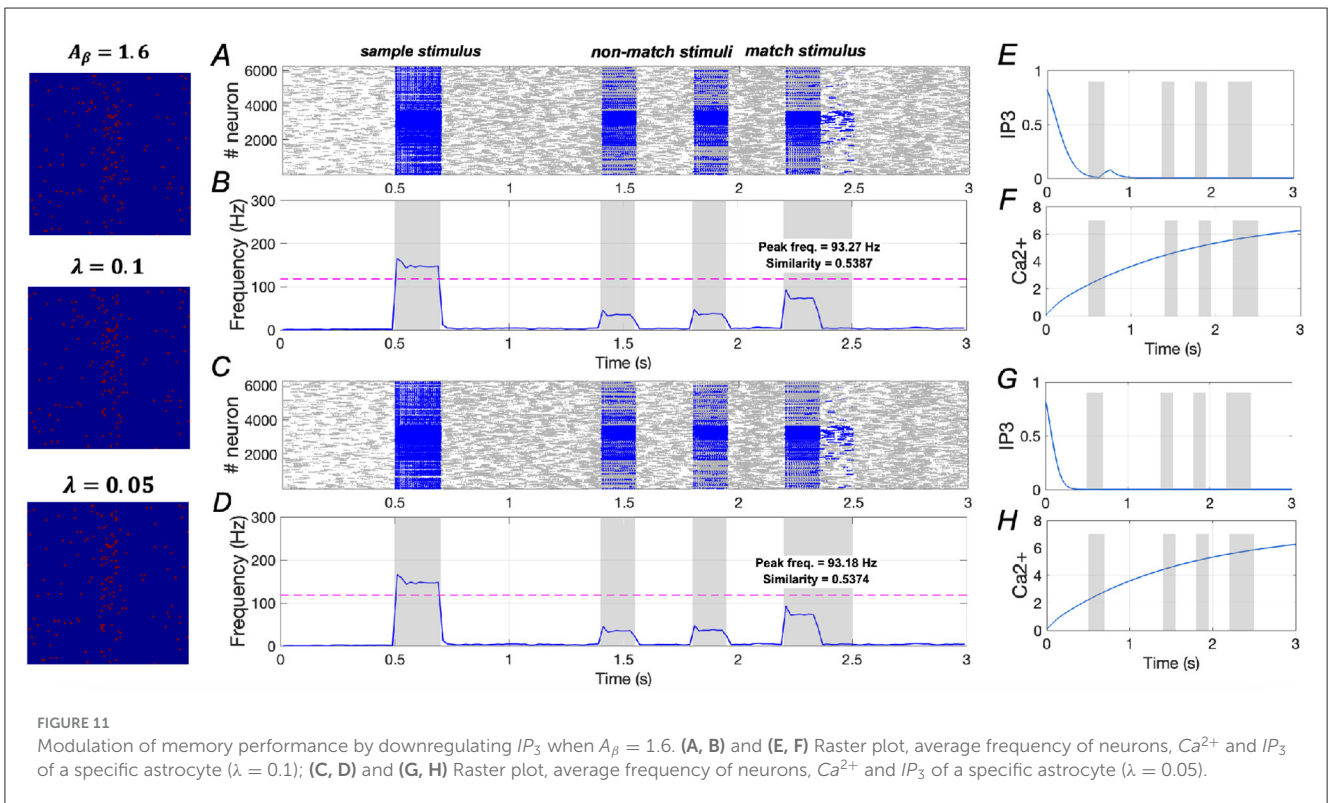
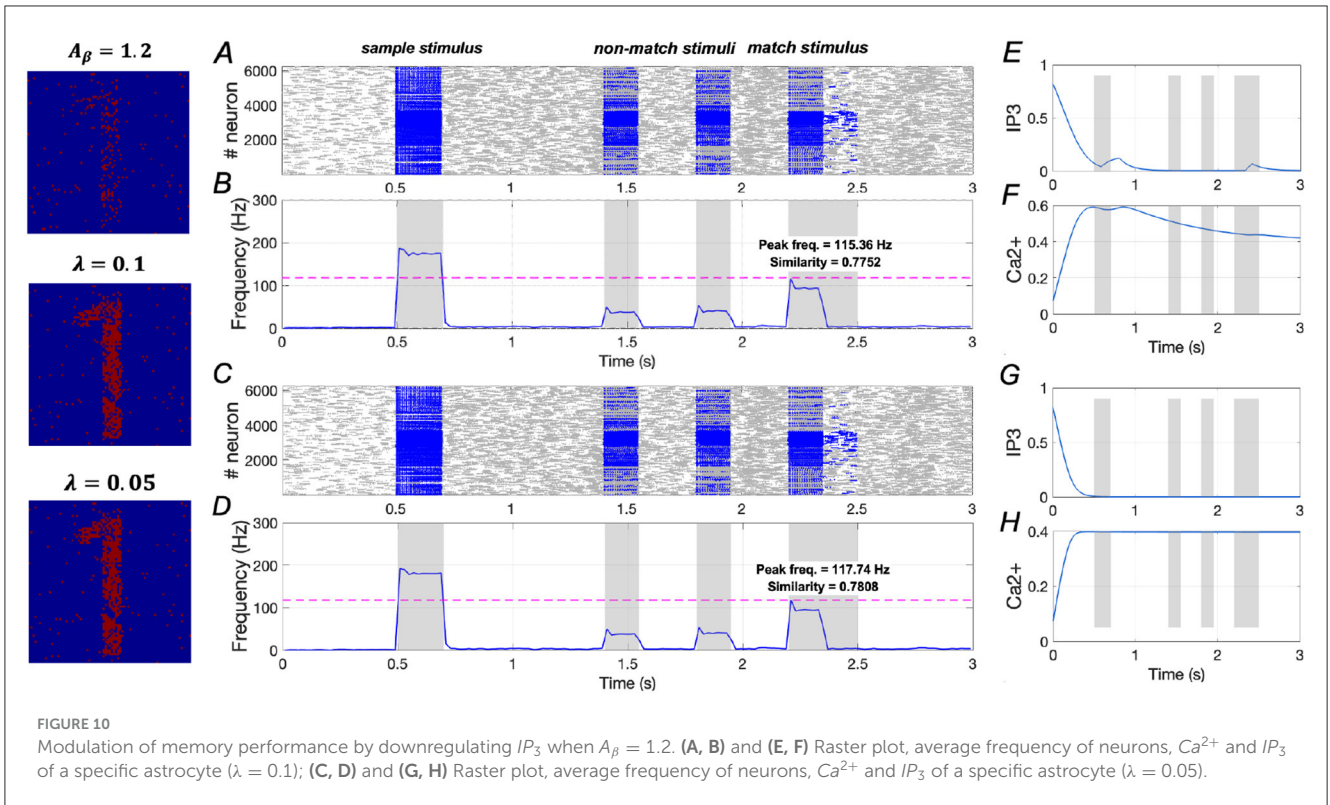
FIGURE 9 Responses of a stimulus-specific neuron and corresponding astrocyte in the presence of $A\beta$ ($A\beta = 1.6$). **(A, B)** Spike train of a specific neuron and the amount of glutamate (G) it releases, respectively; **(C, D)** Ca^{2+} signals and IP_3 values of an astrocyte which has synaptic connection with the specific neuron.

frequency increases from 98.98 Hz to 117.74 Hz, showing a 19.0% increase. These findings suggest that downregulation of IP_3 activation can significantly enhance WM performance under mild AD conditions.

However, in **Figure 11**, under the condition of $A\beta = 1.6$ (severe AD), both $\lambda = 0.1$ and $\lambda = 0.05$ show minimal effects on similarity and peak frequency. This indicates that downregulating IP_3 activation does not improve WM performance in severe AD, underscoring the necessity for a dual-target modulation strategy to achieve full recovery in severe AD patients.

3.4 Restoring WM network performance by downregulating IP_3 activation and upregulating SERCA activation

The effects of upregulating *SERCA* activation on WM performance are illustrated in **Figure 12**. In mild AD conditions, when $\gamma = 1.25$, similarity increases from 0.5832 to 0.6132, reflecting a $\sim 5.1\%$ increase, and peak frequency rises from 98.98 Hz to 101.58 Hz, a $\sim 2.6\%$ increase. However, when $\gamma = 2.0$, similarity increases from 0.5832 to 0.7710, representing a



~32.2% increase, while peak frequency rises from 98.98 Hz to 114.06 Hz, a ~ 15.2% increase (see [Supplementary Figure 19](#)). The corresponding variations in the Ca^{2+} signal for $\gamma = 1.25$ is shown in [Figure 12B](#).

Moreover, simultaneously altering the activations of IP_3 and $SERCA$ significantly enhances WM performance. Specifically, similarity rises from 0.5832 to 0.8105, a ~39.0% increase, and peak frequency increases from 98.98 Hz to 124.06 Hz,

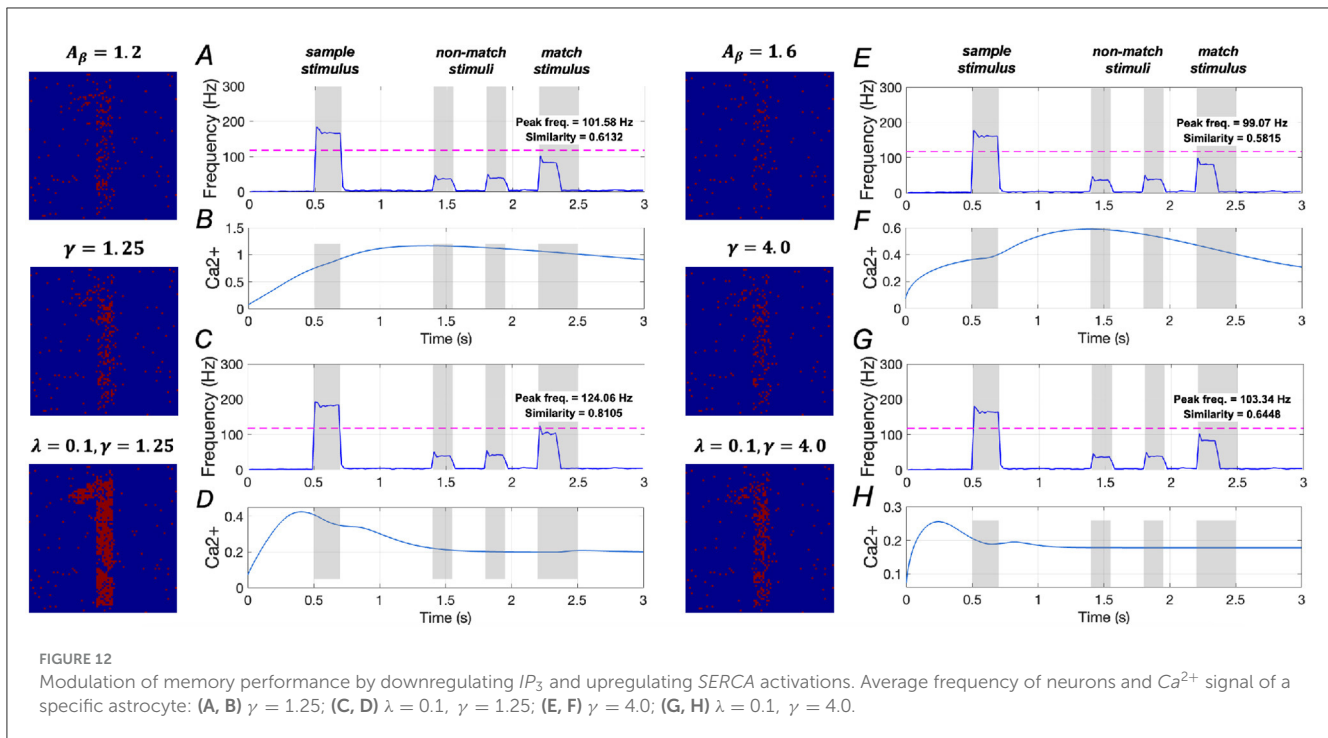


FIGURE 12 Modulation of memory performance by downregulating IP_3 and upregulating $SERCA$ activations. Average frequency of neurons and Ca^{2+} signal of a specific astrocyte: (A, B) $\gamma = 1.25$; (C, D) $\lambda = 0.1, \gamma = 1.25$; (E, F) $\gamma = 4.0$; (G, H) $\lambda = 0.1, \gamma = 4.0$.

reflecting a $\sim 25.3\%$ increase. These findings suggest that concurrently downregulating IP_3 activation while upregulating $SERCA$ activation plays a crucial role in restoring WM under mild AD conditions.

In Figures 12E–H, the model results for severe AD conditions indicate that upregulating $SERCA$ activation has minimal impact on WM performance. Additionally, simultaneous changes to the activations of IP_3 and $SERCA$ show only slight improvements in WM performance. These results imply that simply regulating intracellular calcium levels is insufficient to effectively restore WM performance in severe AD conditions.

3.5 Test the modulatory roles of IP_3 and $SERCA$ using other two sample stimuli

To evaluate the general applicability of our network model, we conducted two additional experiments by changing the sample stimulus to two other digit stimuli: “2” and “7”.

3.5.1 Model evaluation using digit “2” as sample stimulus

Results demonstrated in Figure 13 indicate that the similarity of neuronal responses to the sample and match stimuli reaches ~ 0.8975 , with the peak frequency of neurons responding to the match stimulus being comparable to that of neurons responding to the sample stimulus.

The effects of downregulating IP_3 activation and upregulating $SERCA$ activation on WM performance are illustrated in Figures 14A–D. In mild AD conditions, when $\lambda = 0.1$, similarity increases from 0.5680 to 0.7559, representing a $\sim 33.1\%$ increase,

and peak frequency rises from 107.80 Hz to 125.24 Hz, a $\sim 16.2\%$ increase. When $\gamma = 1.25$, similarity increases from 0.5680 to 0.5991 ($\sim 5.5\%$ increase), and peak frequency rises from 107.80 Hz to 111.06 Hz ($\sim 3.0\%$ increase). When both $\lambda = 0.1$ and $\gamma = 1.25$ are applied, similarity increases from 0.5680 to 0.8016 ($\sim 41.1\%$), and peak frequency rises from 107.80 Hz to 136.29 Hz ($\sim 26.4\%$). These findings suggest that simultaneously downregulating IP_3 activation and upregulating $SERCA$ activation plays a crucial role in restoring WM under mild AD conditions, consistent with the results observed under the sample stimulus “1”.

In severe AD conditions, the model results shown in Figures 14E–H demonstrate that manipulating the activation of IP_3 and $SERCA$, either separately or simultaneously, does not significantly improve memory performance. These findings imply that the WM performance in severe AD cannot be effectively restored solely by regulating intracellular calcium levels, aligning with the conclusions drawn under the sample stimulus “1”.

3.5.2 Model evaluation using digit “7” as sample stimulus

The trends in similarity and peak frequency under sample stimulus “7” are consistent with those observed for sample stimuli “1” and “2”. Specifically, under sample stimulus “7”, the similarity of neuronal responses to the sample and match stimuli reaches ~ 0.8629 , with the peak frequency of neurons responding to the match stimulus being comparable to that of neurons responding to the sample stimulus (Figure 15).

The effects of downregulating IP_3 activation and upregulating $SERCA$ activation on WM performance are illustrated in

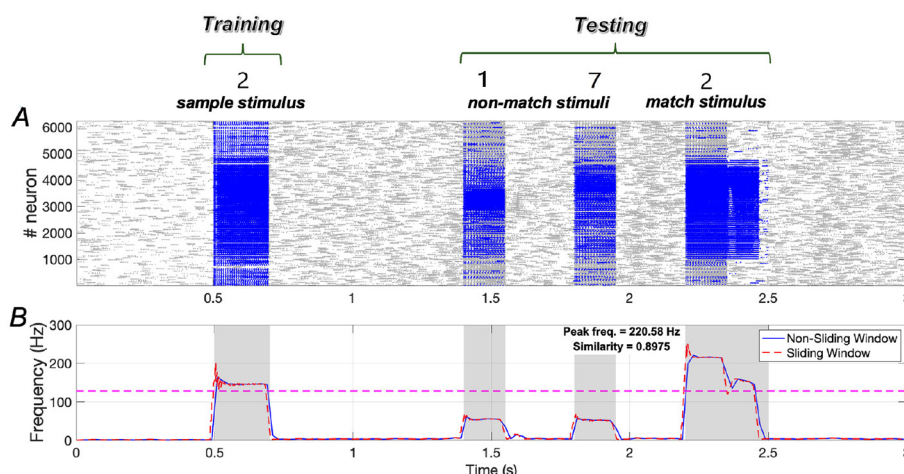


FIGURE 13 Neuronal responses in the WM network when the sample stimulus image is “2”. (A) Raster plots of spikes for all the neurons during different phases; (B) Average frequencies of stimulus-specific neurons using different time windows, respectively (bin = 20 ms).

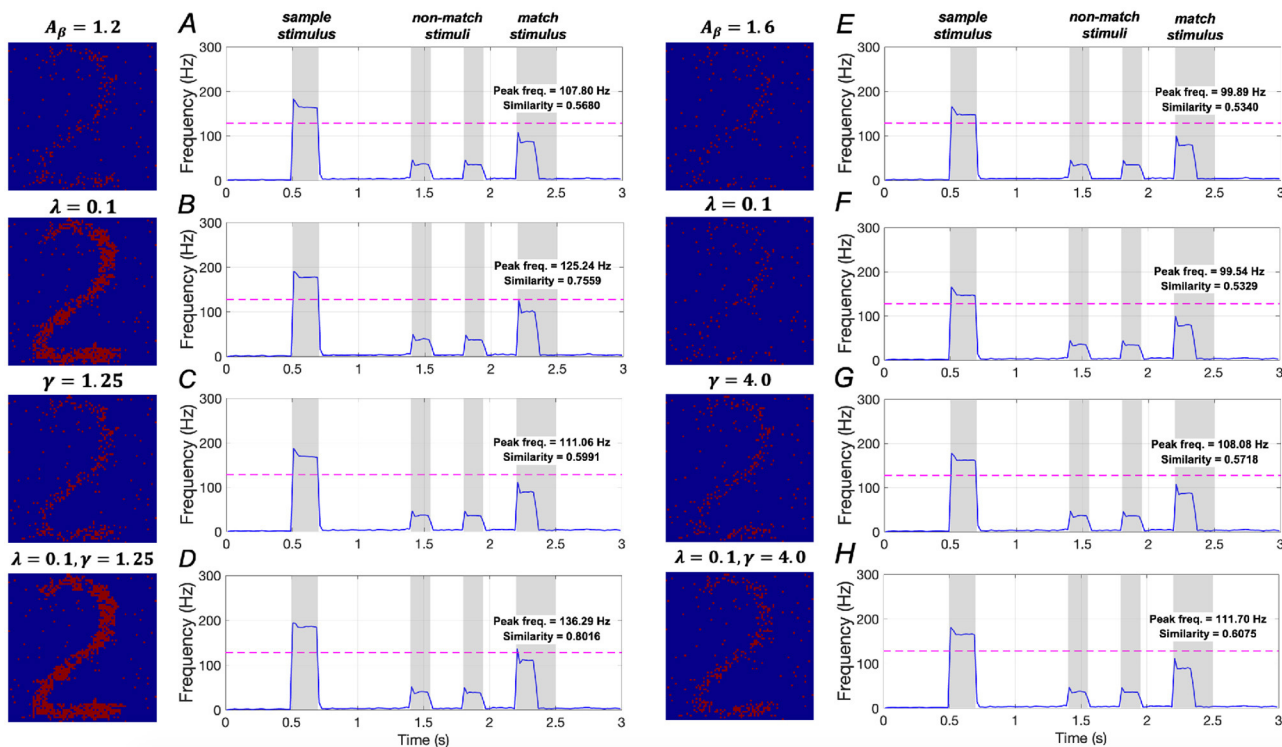


FIGURE 14 Modulation of memory performance when the sample stimulus image is “2”. Average frequency of neurons: (A) AD condition ($A_{\beta} = 1.2$); (B) $\lambda = 0.1$; (C) $\gamma = 1.25$; (D) $\lambda = 0.1, \gamma = 1.25$; (E) AD condition ($A_{\beta} = 1.6$); (F) $\lambda = 0.1$; (G) $\gamma = 4.0$; (H) $\lambda = 0.1, \gamma = 4.0$.

Figures 16A–D. In mild AD conditions, when $\lambda = 0.1$, similarity increases by $\sim 29.3\%$ (from 0.5504 to 0.7117), and peak frequency rises by $\sim 18.0\%$ (from 96.42 Hz to 113.76 Hz). These results suggest that simultaneously downregulating IP_3 activation and upregulating $SERCA$ activation plays a crucial role in restoring WM in mild AD conditions, consistent with the findings under sample stimulus “1”.

increases significantly by $\sim 37.7\%$ (from 0.5504 to 0.7577), and peak frequency rises by $\sim 18.0\%$ (from 96.42 Hz to 113.76 Hz). These results suggest that simultaneously downregulating IP_3 activation and upregulating $SERCA$ activation plays a crucial role in restoring WM in mild AD conditions, consistent with the findings under sample stimulus “1”.

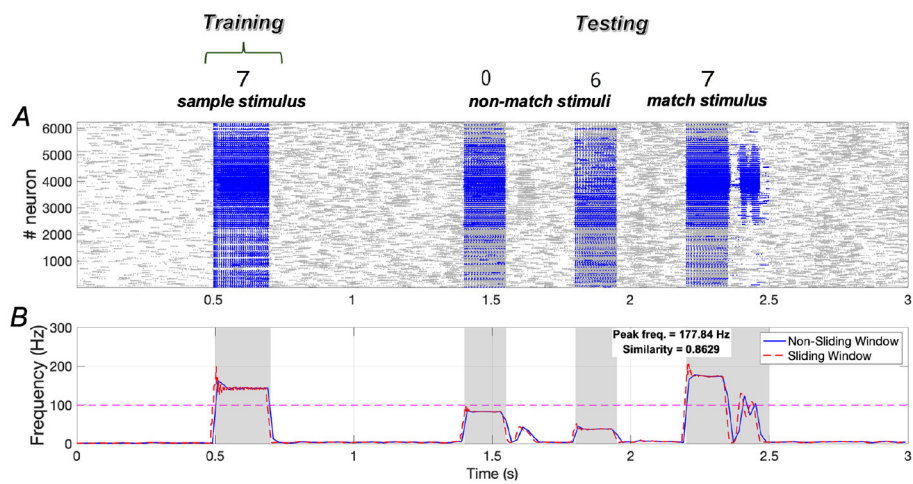


FIGURE 15
Neuronal responses in the WM network when the sample stimulus image “7”. (A) Raster plots of spikes for all the neurons during different phases; (B) Average frequencies of stimulus-specific neurons using different time windows, respectively (bin = 20 ms).

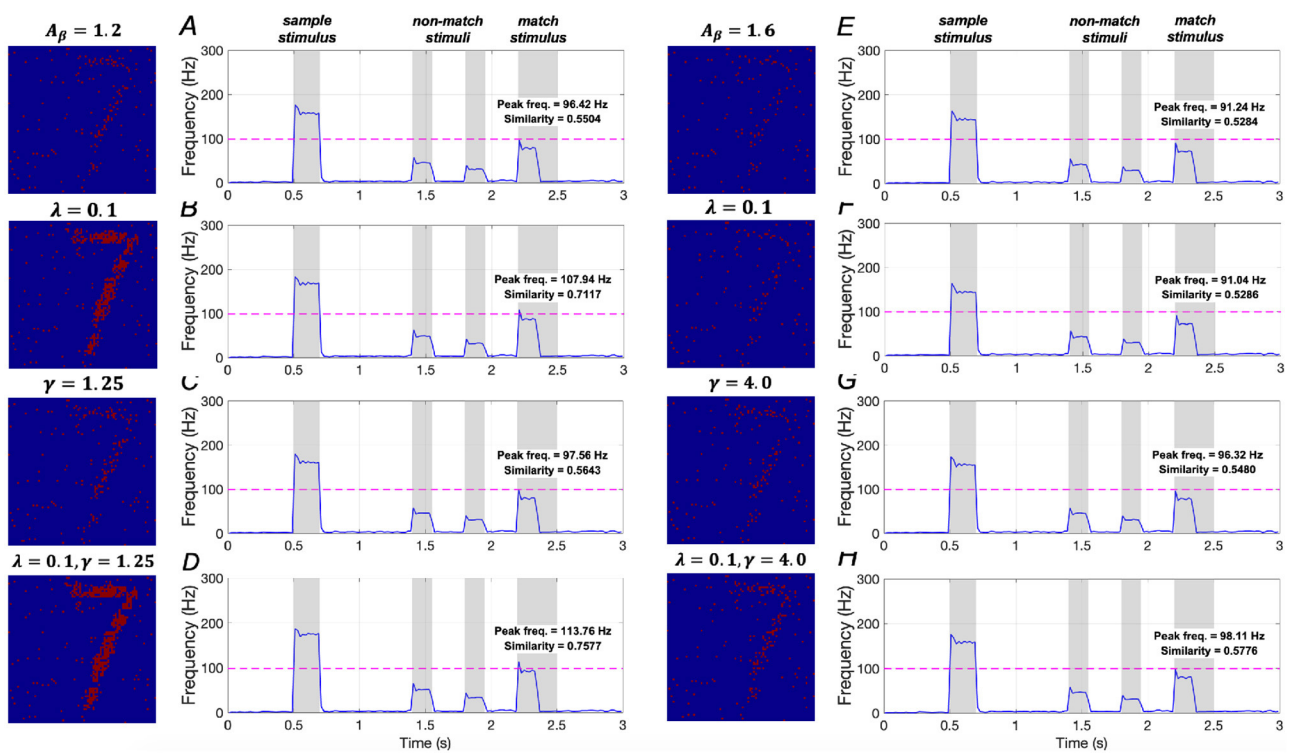


FIGURE 16
Modulation of memory performance when the sample stimulus image is “7”. Average frequency of neurons: (A) AD condition ($A_\beta = 1.2$); (B) $\lambda = 0.1$; (C) $\gamma = 1.25$; (D) $\lambda = 0.1, \gamma = 1.25$; (E) AD condition ($A_\beta = 1.6$); (F) $\lambda = 0.1$; (G) $\gamma = 4.0$; (H) $\lambda = 0.1, \gamma = 4.0$.

Model results for severe AD conditions, shown in Figures 16E–H, demonstrate that manipulating the activations of IP_3 and $SERCA$, either separately or together, does not significantly impact memory performance. There results indicating that WM performance in severe AD cannot be effectively restored by merely regulating intracellular calcium levels, aligning with the conclusions drawn from sample stimulus “1”.

4 Discussions

In this study, we developed a computational model comprising spiking neurons and non-spiking astrocytes to explore how intracellular calcium homeostasis affects WM performance under $A\beta$ -induced AD conditions. Quantitative measures, represented by similarity and peak frequency, indicate that manipulating IP_3

receptor activation and *SERCA* pump activity can significantly enhance memory performance in mild AD conditions. However, minimal effects on performance are observed in severe AD conditions when altering IP_3 and *SERCA* activation. Evaluations using two additional sample stimuli further confirm the general applicability of our network model.

Several previous experimental findings support our proposed modulation strategies of downregulating IP_3 and upregulating *SERCA* as physiologically realistic (Green et al., 2008; Krajnak and Dahl, 2018; Kumar et al., 2015). For instance, mGluR5 antagonists, such as MPEP and fenobam, can pharmacologically reduce IP_3 production by blocking metabotropic glutamate receptor 5 (Kumar et al., 2015). These drugs have been shown to effectively reduce synaptic hyperexcitability and improve memory deficits in mouse models of AD, aligning with our model predictions. Additionally, enhancing *SERCA* pump efficiency has been explored through *SERCA2a* gene therapy in cardiac disease models (Kranias and Hajjar, 2012), where improved calcium handling restores cellular function. While *SERCA* upregulation has not been extensively tested in neuronal contexts, pharmacological activators and gene delivery vectors present promising avenues. Together, these strategies offer a translationally relevant approach to restore calcium homeostasis and potentially reverse early WM damage in $A\beta$ -induced mild AD conditions.

Despite the effectiveness of our model in characterizing WM formation and restoration, several limitations still need to be addressed.

4.1 Model components in the network

First, our network model includes only excitatory neurons, overlooking the crucial role of inhibitory interneurons, which are essential for synchronizing network rhythms and preventing overexcitability. Future studies should incorporate inhibitory interneurons to enhance the realism of the memory model. Second, the astrocyte model is based on mean-field approximations, averaging calcium responses across compartments (Bazargani and Attwell, 2016). This approach simplifies the intricate spatial signaling seen in actual astrocytes, particularly in presynaptic domains. Integrating spatially distinct, cell-type-specific mechanisms would enhance the model's fidelity and biological relevance for future laboratory research.

4.2 $A\beta$ and other hypotheses

In recent decades, the pathogenesis of AD has received considerable attention, leading to several prominent hypotheses: (1) Amyloid Hypothesis ($A\beta$): This hypothesis suggests that neuronal damage in AD patients arises from abnormalities in the processing of amyloid precursor protein (APP) and the subsequent accumulation of $A\beta$ (Hampel et al., 2021). (2) Cholinergic Hypothesis: Supported by experimental observations, this hypothesis highlights a significant reduction in choline acetyltransferase, the enzyme responsible for synthesizing acetylcholine (ACh), in the amygdala, cortex, and hippocampus

of postmortem brains from AD patients (Chen et al., 2022). (3) Glutamate Toxicity Hypothesis: This hypothesis is based on evidence of a marked reduction in the binding of 1-[3H] glutamate in the brains of individuals with AD (Maragos et al., 1987). (4) Tau Hypothesis: This hypothesis is grounded in the observation of aggregates of misfolded tau proteins present in the brains of AD patients (Frost et al., 2009).

While these four hypotheses aim to elucidate the pathophysiological basis of AD, it is important to recognize that the triggers associated with these hypotheses likely do not operate in isolation and may interact synergistically (Patow et al., 2023). In this study, we focused solely on AD conditions induced by $A\beta$ accumulation. Future research should also examine AD conditions triggered by other significant factors.

4.3 Synaptic plasticity in WM network

Plasticity is a well-documented phenomenon at nearly all synapses in the brain, encompassing various types such as short-term plasticity, long-term plasticity (including long-term potentiation and long-term depression), Hebbian learning, and spike-timing-dependent plasticity (STDP). Moreover, synaptic plasticity is believed to play a critical role in the formation and storage of WM (Froudast-Walsh et al., 2018; Huang and Wei, 2021). In this study, however, the performance of the WM network is driven solely by intracellular calcium dynamics, without incorporating mechanisms of synaptic plasticity. Therefore, a potential extension of our network model could involve integrating plasticity mechanisms to explore changes in synaptic weights among cells.

4.4 Functions of $A\beta$ at the genetic level

Our network model operates at the cellular level, while the specific mechanisms of $A\beta$ function predominantly occur at the genetic level. For example, Hao and Friedman developed a mathematical model that outlines the $A\beta$ aggregation process in detail, including production, clearance, and degradation (Hao and Friedman, 2016). Mustafa et al. created a two-compartment diffusion model to examine the effects of $A\beta$ on the acetylcholine neurocycle, incorporating a differential equation to characterize changes in $A\beta$ levels (Mustafa et al., 2021). Similarly, Chamberland et al. proposed a multiscale model consisting of 19 ordinary differential equations to analyze the progression of AD, introducing equations for both intracellular and extracellular $A\beta$ (Chamberland et al., 2024). Models that focus on $A\beta$ at the genetic level may offer a more accurate representation of its dynamic variations. Therefore, future modeling studies on $A\beta$ -related AD generation and progression should incorporate more genetic-level components.

4.5 Other types of memory impairments

Memory impairments are common symptoms observed in the brains of AD patients. Alongside deficits in WM, other

types of memory, such as short-term, episodic, and semantic memories (Jahn, 2013), are also affected during the progression of AD. Furthermore, various memory-related symptoms, including sleep disturbances (Pathmanathan et al., 2025) and accelerated long-term forgetting (Stamate et al., 2020), have been observed. Recent years have seen the development of computational models addressing these symptoms. For example, Horn et al. constructed a biologically motivated Hopfield model to investigate how the interplay between synaptic deletion and compensation influences memory deterioration patterns (Horn et al., 1993). Razi et al. built a network model of coupled cortical columns to explore the propagation modes between sleep and wakefulness (Razi et al., 2021). Additionally, Murre et al. introduced a mathematical model to analyze the dynamics of forgetting and amnesia, applying their findings to experimental observations from mice, rats and monkeys (Murre et al., 2013). Given this context, future computational studies could integrate these model explorations with our spiking network model to investigate potential therapeutic targets for these symptoms under AD conditions.

Data availability statement

The original contributions presented in the study are included in the article/Supplementary material, further inquiries can be directed to the corresponding author.

Author contributions

ZH: Writing – review & editing, Software, Writing – original draft, Conceptualization, Visualization, Data curation, Methodology. LW: Validation, Conceptualization, Investigation, Writing – review & editing, Supervision, Resources.

References

- Bazargani, N., and Attwell, D. (2016). Astrocyte calcium signaling: the third wave. *Nat. Neurosci.* 19, 182–189. doi: 10.1038/nn.4201
- Bertsch, M., Franchi, B., Marcello, N., Tesi, M. C., and Tosin, A. (2017). Alzheimer's disease: a mathematical model for onset and progression. *Math. Med. Biol.* 34, 193–214. doi: 10.1093/imammb/dqw003
- Brejijeh, Z., and Karaman, R. (2020). Comprehensive review on Alzheimer's disease: causes and treatment. *Molecules* 25:5789. doi: 10.3390/molecules25245789
- Chamberland, É., Moravveji, S., Doyon, N., and Duchesne, S. (2024). A computational model of Alzheimer's disease at the nano, micro, and macroscales. *Front. Neuroinform.* 18:1348113. doi: 10.3389/fninf.2024.1348113
- Chen, Z. R., Huang, J. B., Yang, S. L., and Hong, F. F. (2022). Role of cholinergic signaling in Alzheimer's disease. *Molecules* 27:1816. doi: 10.3390/molecules27061816
- Fani, G., Mannini, B., Vecchi, G., Cascella, R., Cecchi, C., Dobson, C. M., et al. (2021). A β oligomers dysregulate calcium homeostasis by mechanosensitive activation of AMPA and NMDA receptors. *ACS Chem. Neurosci.* 12, 766–781. doi: 10.1021/acchemneuro.0c00811
- Farhy-Tselnicker, I., and Allen, N. J. (2018). Astrocytes, neurons, synapses: a tripartite view on cortical circuit development. *Neural Dev.* 13:7. doi: 10.1186/s13064-018-0104-y
- Frost, B., Jacks, R. L., and Diamond, M. I. (2009). Propagation of tau misfolding from the outside to the inside of a cell. *J. Biol. Chem.* 284, 12845–12852. doi: 10.1074/jbc.M808759200
- Froudust-Walsh, S., López-Barroso, D., Torres-Prioris, M. J., Crosson, P. L., and Berthier, M. L. (2018). Plasticity in the working memory system: life span changes and response to injury. *Neuroscientist* 24, 261–276. doi: 10.1177/1073858417717210
- Gordleeva, S. Y., Tsybina, Y. A., Krivososov, M., Ivanchenko, M. V., Zaikin, A. A., Kazantsev, V. B., et al. (2021). Modeling working memory in a spiking neuron network accompanied by astrocytes. *Front. Cell Neurosci.* 15:631485. doi: 10.3389/fncel.2021.631485
- Green, K. N., Demuro, A., Akbari, Y., Hitt, B. D., Smith, I. F., Parker, I., et al. (2008). SERCA pump activity is physiologically regulated by presenilin and regulates amyloid β production. *J. Cell Biol.* 181, 1107–1116. doi: 10.1083/jcb.200706171
- Hampel, H., Hardy, J., Blennow, K., Chen, C., Perry, G., Kim, S. H., et al. (2021). The amyloid- β pathway in Alzheimer's disease. *Mol. Psychiatry* 26, 5481–5503. doi: 10.1038/s41380-021-01249-0
- Hao, W. R., and Friedman, A. (2016). Mathematical model on Alzheimer's disease. *BMC Syst. Biol.* 10:108. doi: 10.1186/s12918-016-0348-2
- Helal, M., Hingant, E., Pujo-Menjouet, L., and Webb, G. F. (2014). Alzheimer's disease: analysis of a mathematical model incorporating the role of prions. *J. Math. Biol.* 69, 1207–1235. doi: 10.1007/s00285-013-0732-0
- Helal, M., Igel-Egalon, A., Lakmeche, A., Mazzocco, P., Perrillat-Mercerot, A., Pujo-Menjouet, L., et al. (2019). Stability analysis of a steady state of a model describing Alzheimer's disease and interactions with prion proteins. *J. Math. Biol.* 78, 57–81. doi: 10.1007/s00285-018-1267-1

Funding

The author(s) declare that no financial support was received for the research and/or publication of this article.

Conflict of interest

The authors declare that the research was conducted in the absence of any commercial or financial relationships that could be construed as a potential conflict of interest.

Generative AI statement

The author(s) declare that no Gen AI was used in the creation of this manuscript.

Publisher's note

All claims expressed in this article are solely those of the authors and do not necessarily represent those of their affiliated organizations, or those of the publisher, the editors and the reviewers. Any product that may be evaluated in this article, or claim that may be made by its manufacturer, is not guaranteed or endorsed by the publisher.

Supplementary material

The Supplementary Material for this article can be found online at: <https://www.frontiersin.org/articles/10.3389/fncom.2025.1643547/full#supplementary-material>

- Horn, D., Ruppin, E., Usher, M., and Herrmann, M. (1993). Neural network modeling of memory deterioration in Alzheimer's disease. *Neural Comput.* 5, 736–749. doi: 10.1162/neco.1993.5.5.736
- Huang, Q. S., and Wei, H. (2021). A computational model of working memory based on spike-timing-dependent plasticity. *Front. Comput. Neurosci.* 15:630999. doi: 10.3389/fncom.2021.630999
- Izhikevich, E. M. (2003). Simple model of spiking neurons. *IEEE Trans. Neural Netw.* 14, 1569–1572. doi: 10.1109/TNN.2003.820440
- Jahn, H. (2013). Memory loss in Alzheimer's disease. *Dialogues Clin. Neurosci.* 15, 445–454. doi: 10.31887/DCNS.2013.15.4/hjahn
- Khoshkhou, M., and Montakhab, A. (2018). Beta-rhythm oscillations and synchronization transition in network models of Izhikevich neurons: effect of topology and synaptic type. *Front. Comput. Neurosci.* 12:59. doi: 10.3389/fncom.2018.00059
- Kim, A. Y., Jerdi, S. A., MacDonald, R., and Triggie, C. R. (2024). Alzheimer's disease and its treatment – yesterday, today and tomorrow. *Front. Pharmacol.* 15:1399121. doi: 10.3389/fphar.2024.1399121
- Kimelberg, H. K., and Nedergaard, M. (2010). Functions of astrocytes and their potential as therapeutic targets. *Neurotherapeutics.* 7, 338–353. doi: 10.1016/j.nurt.2010.07.006
- Krajnak, K., and Dahl, R. (2018). A new target for Alzheimer's disease: a small molecule SERCA activator is neuroprotective *in vitro* and improves memory and cognition in APP/PS1 mice. *Bioorg. Med. Chem. Lett.* 28, 1591–1594. doi: 10.1016/j.bmcl.2018.03.052
- Kranias, E. G., and Hajjar, R. J. (2012). Modulation of cardiac contractility by the phospholamban/ SERCA2a regulatome. *Circ. Res.* 110, 1646–1660. doi: 10.1161/CIRCRESAHA.111.259754
- Kumar, A., Dhull, D. K., and Mishra, P. S. (2015). Therapeutic potential of mGluR5 targeting in Alzheimer's disease. *Front. Neurosci.* 9:215. doi: 10.3389/fnins.2015.00215
- Latulippe, J., Lotito, D., and Murby, D. (2018). A mathematical model for the effects of amyloid beta on intracellular calcium. *PLoS ONE* 13:e0202503. doi: 10.1371/journal.pone.0202503
- Ma, T., and Klann, E. (2012). Amyloid β : linking synaptic plasticity failure to memory disruption in Alzheimer's disease. *J. Neurochem.* 120, 140–148. doi: 10.1111/j.1471-4159.2011.07506.x
- Maragos, W. F., Chu, D. C., Young, A. B., D'Amato, C. J., and Penney Jr, J. B. (1987). Loss of hippocampal [3H]TCP binding in Alzheimer's disease. *Neurosci. Lett.* 74, 371–376. doi: 10.1016/0304-3940(87)90326-0
- Mongillo, G., Barak, O., and Tsodyks, M. (2008). Synaptic theory of working memory. *Science* 319, 1543–1546. doi: 10.1126/science.1150769
- Moravveji, S., Doyon, N., Mashreghi, J., and Duchesne, S. (2024). A scoping review of mathematical models covering Alzheimer's disease progression. *Front. Neuroinform.* 18:1281656. doi: 10.3389/fninf.2024.1281656
- Murre, J. M., Chessa, A. G., and Meeter, M. (2013). A mathematical model of forgetting and amnesia. *Front. Psychol.* 4:76. doi: 10.3389/fpsyg.2013.00076
- Mustafa, I., Awad, A., Fgaier, H., Mansur, A., and Elkamel, A. (2021). Compartmental modeling and analysis of the effect of β -amyloid on acetylcholine neurocycle via choline leakage hypothesis. *Comput. Chem. Eng.* 145:107165. doi: 10.1016/j.compchemeng.2020.107165
- Neher, E., and Sakaba, T. (2008). Multiple roles of calcium ions in the regulation of neurotransmitter release. *Neuron* 59, 861–872. doi: 10.1016/j.neuron.2008.08.019
- Pathmanathan, J., Westover, M. B., Sivakumaran, S., Donoghue, J., and Puryear, C. B. (2025). The role of sleep in Alzheimer's disease: a mini review. *Front. Neurosci.* 19:1428733. doi: 10.3389/fnins.2025.1428733
- Patow, G., Stefanovski, L., Ritter, P., Deco, G., and Kobeleva, X. (2023). Whole-brain modeling of the differential influences of amyloid-beta and tau in Alzheimer's disease. *Alzheimers Res. Ther.* 15:210. doi: 10.1186/s13195-023-01349-9
- Poling, A., Morgan-Paisley, K., Panos, J. J., Kim, E., O'Hare, E., Cleary, J. P., et al. (2008). Oligomers of the amyloid-beta protein disrupt working memory: confirmation with two behavioral procedures. *Behav. Brain Res.* 193, 230–234. doi: 10.1016/j.bbr.2008.06.001
- Puri, I. K., and Li, L. W. (2010). Mathematical modeling for the pathogenesis of Alzheimer's disease. *PLoS ONE* 5:e15176. doi: 10.1371/journal.pone.0015176
- Razi, F., Moreno-Bote, R., and San Cristóbal, B. (2021). Computational modeling of information propagation during the sleep-walking cycle. *Biology* 10:945. doi: 10.3390/biology10100945
- Stamate, A., Logie, R. H., Baddeley, A. D., and Sala, S. D. (2020). Forgetting in Alzheimer's disease: is it fast? Is it affected by repeated retrieval? *Neuropsychologia* 138:107351. doi: 10.1016/j.neuropsychologia.2020.107351
- Toglia, P., Demuro, A., Mak, D. D., and Ullah, G. (2018). Data-driven modeling of mitochondrial dysfunction in Alzheimer's disease. *Cell Calcium* 76, 23–35. doi: 10.1016/j.ceca.2018.09.003
- Vermma, M., Lizama, B. N., and Chu, C. T. (2022). Excitotoxicity, calcium and mitochondria: a triad in synaptic neurodegeneration. *Transl. Neurodegener.* 11:3. doi: 10.1186/s40035-021-00278-7
- Wagner, J., Fall, C. P., Hong, F., Sims, C. E., Allbritton, N. L., Fontanilla, R. A., et al. (2004). A wave of IP₃ production accompanies the fertilization Ca²⁺ wave in the egg of the frog, *Xenopus laevis*: theoretical and experimental support. *Cell Calcium* 35, 433–447. doi: 10.1016/j.ceca.2003.10.009